Method of High Signal-to-Noise Ratio and Wide Swath SAR Imaging Based on Continuous Pulse Coding

Jingyi Wei, *Student Member, IEEE*, Yachao Li, *Member, IEEE*, Rui Yang, Lianghai Li, and Liang Guo, *Member, IEEE*

***Abstract*—In synthetic aperture radar (SAR), increasing the pulsewidth of signal is an effective way to achieve high signal-to-noise ratio (HSNR) imaging. However, when the pulse repetition frequency (PRF) is fixed, increasing the pulsewidth will reduce the maximum unambiguous swath width of SAR. In order to solve this contradiction, a method based on continuous pulse coding (CPC) which increases the average transmit power by multiple pulses with varying high PRF is proposed in this article. Due to the small interval between pulses, the echo will have range ambiguity and occlusion problems. To obtain the complete echo, we first use the form of CPC signal and the swath width of radar to construct a linear equation set to model the ambiguous echo of each receiving window. Next, the established linear equations are split according to the distribution law of receiving window. Finally, the echo energy accumulation of multiple pulses is accomplished by solving the split sublinear equations. Therefore, the echo with both swath width corresponding to narrow pulse and HSNR corresponding to wide pulse is obtained to realize HSNR and wide swath SAR imaging. The experimental results have confirmed the effectiveness of the method proposed in this article.**

***Index Terms*—Continuous pulse coding (CPC), decoding, high signal-to-noise ratio and wide swath (HSNR–WS), synthetic aperture radar (SAR).**

I. Introduction

THE characteristics of synthetic aperture radar (SAR) that can obtain high-resolution imaging of the target regardless of time and weather make SAR has an important application value in military and civilian [1]. The signal-to-noise ratio (SNR) is one of the core indexes that are used to measure the quality of SAR image, which is closely related to the average transmit power of radar [2]. We usually increase the peak power or pulsewidth of the signal to increase the average transmit power of the radar. In this case, the high peak transmit power leads to the complexity of radar equipment as well as the high peak power pulse signal is easily intercepted by other jamming equipment. In addition, the increase of the pulsewidth will reduce the observation area of radar when the pulse repetition frequency (PRF) is fixed.

To obtain high signal-to-noise ratio (HSNR) images without reducing the observation area of SAR, researchers have proposed many methods based on the multiaperture radar. A method to improve the SNR of echo utilizing multiple subaperture coherent accumulation in the pitch dimension was proposed in [3]–[5]. In [6]–[7], an area array SAR system based on two-dimensional (2-D) intrapulse scanning is used to obtain HSNR echo. The method of increasing the SNR of the radar in [8] proposed an azimuth-slow time waveform coding scheme based on Alamouti space–time coding. But the above methods all use multiaperture radar, which will increase the complexity of the radar system.

The improvement of SNR in radar can also be achieved by signal waveform coding. The essence of radar waveform coding is modulating the time, frequency, and phase of the transmitted signal. Different modulation methods have different effects on the performance of the radar system. For example, adding a random initial phase to the pulse signal [9]–[12], adjusting slightly the modulation frequency of signal [13]–[15], or changing the polarity of the modulation frequency rate [16]–[17] using multicarrier signal [18]–[21] are all effective ways to suppress interference. Besides, radar waveform coding method is also applied to clutter suppression [22]–[24], resolution enhancement [25]–[29], and range and azimuth ambiguity suppression [30]–[34]. Wang *et al.* [35] proposed a coding signal composed of multiple pulses transmitted in single-channel SAR. Then, the multiple complete echoes are recovered in a pulse coding signal repetition period, and they are coherently superimposed to improve the SNR of radar echo. But in order to ensure that the max unambiguous swath width of this coding SAR is consistent with traditional SAR, it is necessary to reduce the

Manuscript received November 15, 2021; revised January 25, 2022; accepted February 12, 2022. Date of publication February 24, 2022; date of current version March 16, 2022. This work was supported in part by the National Key R&D Program of China under Grant 2018YFB2202500, in part by the National Natural Science Foundation of China under Grant 62171337, in part by the Key R&D program of Shaanxi Province under Grant 2017KW-ZD-12, in part by the Shaanxi Province Funds for Distinguished Young Youths under Grant S2020-JC-JQ-0056, in part by the National Natural Science Foundation of China under Grant 62101396, and in part by the Fundamental Research Funds for the Central Universities under Grant XJS212205. *(Corresponding author: Yachao Li.)*

Jingyi Wei and Yachao Li are with the National Laboratory of Radar Signal Processing, Xidian University, Xi'an 710071, China, and also with the Collaborative Innovation Center of Information Sensing and Understanding, Xidian University, Xi'an 710071, China (e-mail: jywei@stu.xidian.edu.cn; ycli@mail.xidian.edu.cn).

Rui Yang is with the School of Electronic Engineering, Xidian University, Xi'an 710071, China (e-mail: ruiyang.xidian@gmail.com).

Lianghai Li is with the Beijing Research Institute of Telemetry, Beijing 100076, China (e-mail: 13910323802@163.com).

Liang Guo is with the School of Physics and Optoelectronic Engineering, Xidian University, Xi'an 710071, China (e-mail: lguo@mail.xidian.edu.cn).

Digital Object Identifier 10.1109/JSTARS.2022.3153118

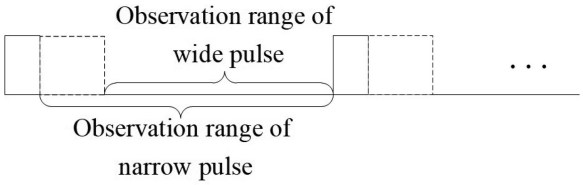

Fig. 1. Schematic diagram of observation range corresponding to different pulse.

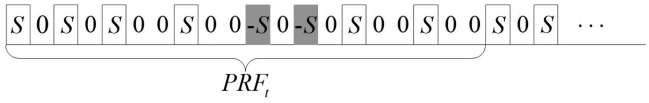

Fig. 2. Model of continuous pulse coding signal.

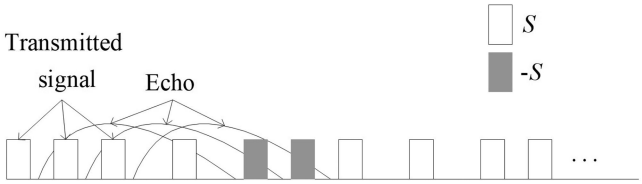

Fig. 3. Echo diagram of continuous pulse coding signal.

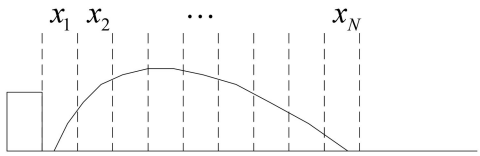

Fig. 4. Diagram of echo blocking.

coding signal repetition frequency, which may cause azimuth Doppler ambiguity of radar due to the undersampling.

For this reason, we introduce a continuous pulse coding (CPC) method in this article, which increases the average transmission power of radar by continuously transmitting pulse train signals. This pulse train signal is composed of narrow pulse signals with varying high PRF. And the contradiction between high average transmit power and wide swath (WS) can be eliminated according to the decoding method to achieve HSNR–WS imaging of SAR. In addition, due to the continuity of the pulse coding signal and the periodicity of the decoding method, compared with the traditional pulse coding method in [35], the CPC method can equivalently increase the azimuth sampling rate and the maximum unambiguous Doppler bandwidth of the radar, so that this new coding method can be applied to radars located on high-speed platforms.

The rest of this article is organized as follows. In Section II, we introduce the mathematical model of CPC signal. In Section III, we analyze and model the echo signal of each receiving window, and elaborate echo recovery. In Section IV, we briefly introduce the basic SAR imaging method, and then make a quantitative analysis of the improvement of SAR image SNR by proposed method. In Section V, the experiment results are shown to verify the effectiveness of proposed method in this article. Finally, Section VI. concludes this article.

II. Model of Continuous Pulse Coding Signal

As shown in Fig. 1, increasing the pulsewidth is an easy way to improve the average transmit power of radar, but it will reduce the observation area of radar. To solve this problem, we propose a new pulse coding method to increase the average transmission power of radar by continuously transmitting pulse train signals composed of narrow pulse signals.

The CPC signal is composed of three symbols, i.e., "0," "S," and "$-S$," whose time widths are all T_p. "S" is a linear frequency modulation (LFM) pulse signal, "0" represents a receiving window and $-S = S \cdot e^{j\pi}$. The transmitting signal of radar can be expressed as

$$\boldsymbol{S}_t = \boldsymbol{D}S \tag{1}$$

where $\boldsymbol{D} = [d_1, d_2 \ldots, d_L]^T$, $d_l = \{0, \pm 1\}$ is determined by the transmitted signal. L is the number of the symbols in $\boldsymbol{S}_t$. $\boldsymbol{D}$ is used to represent the distribution of the symbols in $\boldsymbol{S}_t$.

The radar continuously transmits a pulse train $\boldsymbol{S}_t$, whose period is the time width of the coded signal. Therefore, the repetition frequency of the pulse train in radar can be expressed as

$$\mathrm{PRF}_t = 1/\left(L \cdot T_p\right). \tag{2}$$

As shown in Fig. 2, if the time width of each symbol is 5 μs, the pulse train repetition frequency of radar is 10 kHz according to (2).

As shown in Fig. 3, owing to the short interval of the subpulses in coding signal and the work mode of single-channel radar, the echoes will have ambiguity and occlusion problems. Therefore, it is impossible to directly utilize the echo in Fig. 3 for SAR imaging. In next section, how to recover the complete echoes will be described in detail.

III. Echo Decoding Method of CPC–SAR

Due to the limitation of radar beam width, the echo length corresponding to a subpulse is also limited. Assuming that the longest duration of the target echo corresponding to a single pulse from the beginning to the end of the reception is T, then we can obtain the length N of the echo signal $\boldsymbol{x}$ by rounding up from T/T_p. Therefore, the echo signal is divided into N units, i.e., $x_1, x_2 \ldots, x_N$, which can be shown in Fig. 4.

When the CPC signal is determined, we define M as the total number of receiving windows in the transmitted coding signal, and its size is the product of the number of the receiving windows in one pulse coding signal repetition period and the number of coding signal repetition periods. In addition, define P as the total number of single pulses in the transmitted coding signal, which is the product of the number of single pulses in the repetition period of a pulse coding signal and the number of repetition periods of the coding signal.

Without considering the effect of noise, the following linear equation set $\boldsymbol{Y}$ can be constructed according to the echoes received by the receiving window located at the symbol "0":

$$\boldsymbol{Y} : \boldsymbol{W}\boldsymbol{X} = \boldsymbol{R} \tag{3}$$

where

$$\begin{aligned} \boldsymbol{R} &= [r_1, r_2 \cdots r_M]^T \\ \boldsymbol{X} &= [\boldsymbol{X}_1, \boldsymbol{X}_2, \cdots \boldsymbol{X}_P]^T \\ \boldsymbol{W} &= \begin{bmatrix} \boldsymbol{w}_{11} & \boldsymbol{w}_{12} & \cdots & \boldsymbol{w}_{1P} \\ \boldsymbol{w}_{21} & \boldsymbol{w}_{22} & \cdots & \boldsymbol{w}_{2P} \\ \vdots & \vdots & \ddots & \vdots \\ \boldsymbol{w}_{M1} & \boldsymbol{w}_{M2} & \cdots & \boldsymbol{w}_{MP} \end{bmatrix}. \end{aligned} \tag{4}$$

$\boldsymbol{R}$ represents the aliased target echo received by each receiving window. $\boldsymbol{X}_p$ represents the complete echo of length N corresponding to the pth pulse in the transmitted signal, which can be expressed as

$$\boldsymbol{X}_p = \left[x_{p1}\ x_{p2} \cdots\ x_{pN} \right], p \in [1, P]. \tag{5}$$

$\boldsymbol{W}$ is the observation matrix which depends on the echo length and the form of the CPC signal, where $\boldsymbol{w}_{mp}$ can be expressed as

$$\begin{aligned} \boldsymbol{w}_{mp} &= \left[w_{mp}(1)\ w_{mp}(2) \cdots\ w_{mp}(N) \right] \\ w_{mp}(n) &= \{0, \pm 1\}, m \in [1, M], n \in [1, N], p \in [1, P]. \end{aligned} \tag{6}$$

$w_{mp}(n)$ represents whether there is an nth echo x_{pn} corresponding to the pth pulse in the mth receiving window. If it exists, then according to the phase of the pth pulse, if the phase is 0, the value of $w_{mp}(n)$ is 1, otherwise the value is -1, and if there is no echo x_{pn} in the mth receiving window, the value is 0.

Next, we solve (3) in the following steps:

1) Extract the first Q continuous subequations from (3) to form the subequation group $\boldsymbol{y}_1$

$$\boldsymbol{y}_1 \in \boldsymbol{Y}\ : \boldsymbol{w}_1 \boldsymbol{X} = \boldsymbol{r}_1 \tag{7}$$

where

$$\begin{aligned} \boldsymbol{r}_1 &= [r_1, r_2 \cdots r_Q]^T \\ \boldsymbol{X} &= [\boldsymbol{X}_1, \boldsymbol{X}_2, \cdots \boldsymbol{X}_P]^T \\ \boldsymbol{w}_1 &= \begin{bmatrix} \boldsymbol{w}_{11} & \boldsymbol{w}_{12} & \cdots & \boldsymbol{w}_{1P} \\ \boldsymbol{w}_{21} & \boldsymbol{w}_{22} & \cdots & \boldsymbol{w}_{2P} \\ \vdots & \vdots & \ddots & \vdots \\ \boldsymbol{w}_{Q1} & \boldsymbol{w}_{Q2} & \cdots & \boldsymbol{w}_{QP} \end{bmatrix}. \end{aligned} \tag{8}$$

By observing the element values of the observation matrix $\boldsymbol{w}_1$ in (8), we define two variables $p_{\min}$ and $p_{\max}$, whose values are, respectively, shown as

$$\begin{aligned} p_{\min} &= \min \{p | w_{mp}(n) = \pm 1\}, m \in [1, Q] \\ p_{\max} &= \max \{p | w_{mp}(n) = \pm 1\}, m \in [1, Q] \end{aligned} \tag{9}$$

that is to say, there are the echoes corresponding to the transmitted pulses sequence number between $p_{\min}$ and $p_{\max}$ in these Q receiving windows. Therefore, the observation matrix $\boldsymbol{w}_1$ in (8) can be simplified as

$$\boldsymbol{w}_1 = \begin{bmatrix} 0 & \cdots & 0 & \boldsymbol{w}_{1p_{\min}} & \cdots & \boldsymbol{w}_{1p_{\max}} & 0 & \cdots & 0 \\ 0 & \cdots & 0 & \boldsymbol{w}_{2p_{\min}} & \cdots & \boldsymbol{w}_{2p_{\max}} & 0 & \cdots & 0 \\ \vdots & \ddots & \vdots & \vdots & \ddots & \vdots & \vdots & \ddots & \vdots \\ 0 & \cdots & 0 & \boldsymbol{w}_{Qp_{\min}} & \cdots & \boldsymbol{w}_{Qp_{\max}} & 0 & \cdots & 0 \end{bmatrix}. \tag{10}$$

In order to further simplify (7), we introduce the slant range model of SAR as follows:

$$\begin{aligned} R(t_m; R_0) &= \sqrt{{R_0}^2 + V^2 t_m^2} \\ &\approx R_0 + \frac{1}{2}\frac{V^2}{R_0} t_m^2, t_m \in [-T_s/2, T_s/2] \end{aligned} \tag{11}$$

where $R(t_m; R_0)$ represents the distance from the radar to the target at a certain slow time t_m. R_0 is the shortest distance from the target to the radar. V is the speed of the radar platform. T_s is the time of the synthetic aperture of the radar, which can be calculated by (12)

$$T_s = \Delta\theta \cdot R_0 / V \tag{12}$$

where $\Delta\theta$ is the coherent accumulation angle of SAR.

We define the time interval between the $p_{\min}th$ and $p_{\max}th$ transmission pulses in the CPC signal is Δt_m. Then the echo phase difference $\Delta\phi$ of the echoes corresponding to the $p_{\min}th$ and $p_{\max}th$ transmitted pulses can be expressed as

$$\begin{aligned} \Delta\phi &= 2\left[R(t_m + \Delta t_m; R_0) - R(t_m; R_0)\right] \cdot 2\pi/\lambda \\ &\approx \frac{2\pi}{\lambda} \frac{\left(V^2 \Delta t_m^2 + 2V^2 \Delta t_m t_m\right)}{R_0}, t_m \in [-T_s/2, T_s/2] \end{aligned} \tag{13}$$

where λ is the wavelength of the radar signal. When $t_m = T_s/2$, $\Delta\phi$ has the maximum value. Therefore, the maximum value of $\Delta\phi$ can be calculated by (12) and (13), which can be expressed as

$$\Delta\phi_{\max}(\Delta t_m) = \frac{2\pi}{\lambda}\left(\frac{V^2 \Delta t_m^2}{R_0} + V\Delta\theta\Delta t_m\right). \tag{14}$$

Because the value of Δt_m is generally at the microsecond level, $V^2 \Delta t_m^2 \ll R_0$. Then, (14) can be approximated as

$$\Delta\phi_{\max}(\Delta t_m) \approx \frac{2\pi}{\lambda} V\Delta\theta\Delta t_m. \tag{15}$$

In the traditional SAR imaging algorithm, the classic value of phase compensation accuracy δ_ϕ is $\pi/4$. We use this compensation accuracy as a critical value. When $\Delta\phi_{\max}(\Delta t_m)$ is less than δ_ϕ, we can ignore the phase difference. So we can consider that the echo signals $\boldsymbol{X}_p$ corresponding to the transmitted pulses sequence number between $p_{\min}$ and $p_{\max}$ are approximately equal as shown as

$$\begin{aligned} &\boldsymbol{X}_p = \boldsymbol{X}_{p_{\min}} = \boldsymbol{X}_{p_{\max}}, p \in [p_{\min}, p_{\max}] \\ &\text{s.t. } \Delta\phi_{\max}(\Delta t_m) \le \delta_\phi. \end{aligned} \tag{16}$$

Substituting (16) and (10) into (7), the sublinear equations $\boldsymbol{y}_1$ can be rewritten as

$$\boldsymbol{y}_1 \in \boldsymbol{Y} : \boldsymbol{w}_1 \tilde{\boldsymbol{x}}_1 = \boldsymbol{r}_1 \tag{17}$$

where

$$\boldsymbol{w}_1 = \begin{bmatrix} \sum_{p=p_{\min}}^{p_{\max}} \boldsymbol{w}_{1p} \\ \sum_{p=p_{\min}}^{p_{\max}} \boldsymbol{w}_{2p} \\ \vdots \\ \sum_{p=p_{\min}}^{p_{\max}} \boldsymbol{w}_{Qp} \end{bmatrix}, \tilde{\boldsymbol{x}}_1 = \begin{bmatrix} \tilde{x}_1 \\ \tilde{x}_2 \\ \vdots \\ \tilde{x}_N \end{bmatrix}. \tag{18}$$

The solution of (17) can be written as

$$\tilde{\boldsymbol{x}}_1 = \left(\boldsymbol{w}_1{}^T \boldsymbol{w}_1\right)^{-1} \boldsymbol{w}_1{}^T \boldsymbol{r}_1. \tag{19}$$

By solving (17), we can obtain the complete echo $\tilde{\boldsymbol{x}}_1$ from the aliased echoes in the Q receiving windows. It should be noted that $\tilde{\boldsymbol{x}}_1$ is a generalized concept, which does not correspond to any pulse in the transmitted coding signal. In order to make (17) has a solution, we must ensure that the rank of the observation matrix is greater than or equal to the complete echo length N, which is shown as

$$\text{rank}(\boldsymbol{w}_1) \geq N. \tag{20}$$

1) In $\boldsymbol{Y}$, the continuous Q equations are selected with K as the step size to form a new subequation group $\boldsymbol{y}$ shown in (21). Repeat the above operation until the last equation in $\boldsymbol{Y}$ is selected, and simplify the sublinear equations and estimate the corresponding $\tilde{\boldsymbol{x}}$ according to the operation in step 1

$$\boldsymbol{y} \in \boldsymbol{Y} : \boldsymbol{w}\boldsymbol{X} = \boldsymbol{r} \tag{21}$$

where

$$\boldsymbol{r} = [r_{1+K}, r_{2+K} \cdots r_{Q+K}]^T$$

$$\boldsymbol{X} = [\boldsymbol{X}_1, \boldsymbol{X}_2, \cdots \boldsymbol{X}_P]^T$$

$$\boldsymbol{w} = \begin{bmatrix} \boldsymbol{w}_{(1+K)1} & \boldsymbol{w}_{(1+K)2} & \cdots & \boldsymbol{w}_{(1+K)P} \\ \boldsymbol{w}_{(2+K)1} & \boldsymbol{w}_{(2+K)2} & \cdots & \boldsymbol{w}_{(2+K)P} \\ \vdots & \vdots & \ddots & \vdots \\ \boldsymbol{w}_{(Q+K)1} & \boldsymbol{w}_{(Q+K)2} & \cdots & \boldsymbol{w}_{(Q+K)P} \end{bmatrix}. \tag{22}$$

An equation in (3) represents the aliased echoes of some subpulses in a receiving window. Since the echoes for CPC SAR imaging are no longer the echoes within a long receiving window in each pulse repetition cycle of traditional radar, but the echoes obtained by specific linear operation of multiple echoes distributed in discontinuous narrow receiving windows. Therefore, the PRF_r in the subsequent imaging is determined by the position of the receiving windows selected in the echo recovery rather than by the pulse train repetition frequency PRF_t. In order to effectively perform SAR imaging, the azimuth echoes need to be uniformly sampled. So the selection of K should ensure that the receiving window corresponding to the sublinear equation group is periodically distributed between groups. If the distribution period of each group of receiving windows is T, the equivalent PRF_r can be approximately expressed as

$$\text{PRF}_r = 1/T. \tag{23}$$

Because the number of the echoes recovered in a pulse train repetition period is greater than 1, PRF_r is generally greater than PRF_t. In addition, with the purpose of showing that the CPC method will not reduce the swath width of SAR, the echo length N we set is usually the maximum unambiguous swath width corresponding to the PRF_r calculated by (23) for traditional SAR.

In the proposed coding method, multiple narrow pulses with high PRF are used to replace a wide pulse signal to increase the average transmit power of the radar. By the decoding process, the echoes energy of multiple narrow pulses are accumulated, so that we can recover the echo with both the swath width corresponding to the narrow pulse and the high SNR corresponding to the wide pulse to achieve HSNR–WS imaging of SAR.

Fig. 5(a) and (b), respectively, shows the coding and decoding processes of the CPC method and the traditional coding method when the same coded signal and the same maximum unambiguous swath width are employed in the signal repetition period of the radar.

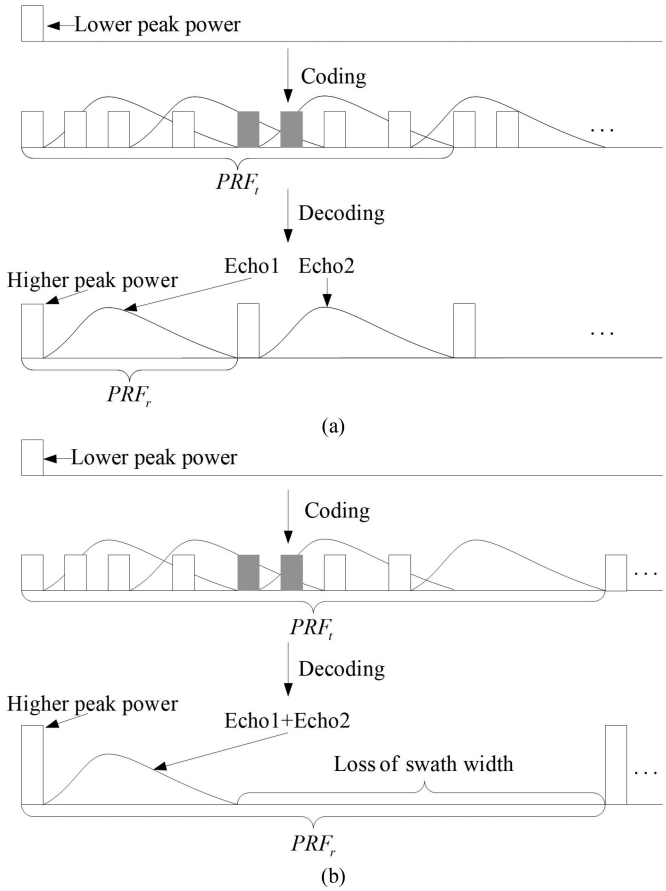

Fig. 5. Schematic diagram of pulse coding and decoding process. (a) Schematic diagram of CPC–SAR. (b) Schematic diagram of traditional coding SAR.

In transmitting and receiving signals, the traditional pulse coding method needs to ensure that the radar receives the whole echo of the last subpulse in the current pulse train repetition period before the next pulse train repetition period. Therefore, as shown in Fig. 5(b), its swath width will be reduced greatly due to transmitting the coded signal for a long time. The proposed coding method does not require that, but continuously transmits the coded signal with the total time width of the pulse coded signal as the period. Therefore, compared with the traditional coding method, the CPC–SAR has larger coding signal repetition frequency PRF_t.

Moreover, due to the continuity of the transmitted signal in CPC–SAR, the proposed method can make the multiple complete target signals recovered in each pulse train repetition period have uniform sampling characteristics in the azimuth direction after decoding. Therefore, we can regard each recovered complete echo as the sampled echo of the CPC–SAR at a certain azimuth moment, which leads to the equivalent azimuth sampling rate PRF_r of CPC–SAR is several times than that of traditional coding SAR. Consequently, it is more easily for traditional coding SAR to occur the problem of spectrum aliasing in azimuth than CPC–SAR.

In summary, the two coding methods both have the ability to improve the SNR of radar echoes due to the high average transmission power, but their differences in the coding and decoding process result in the traditional coding method not having a WS imaging capability.

In the actual imaging process, the design and application of continuous pulse coded signals need to be combined with various radar parameters to achieve the expected imaging effect. The processing flow chart of method for HSNR–WS SAR images based on CPC can be summarized in Fig. 6.

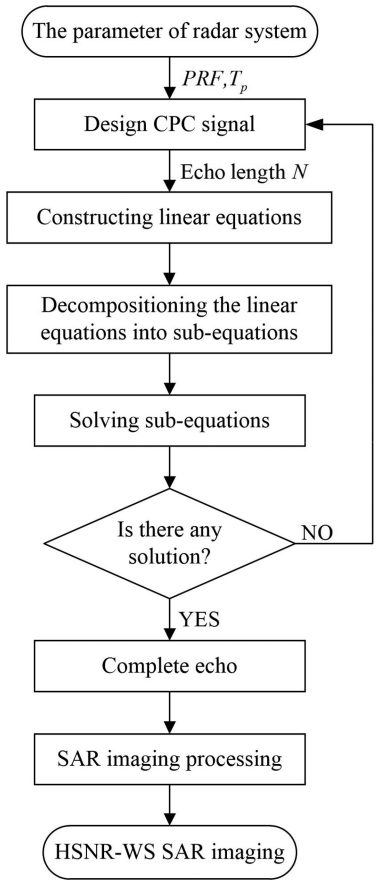

Fig. 6. Procedure of HSNR–WS SAR imaging.

IV. Analysis of SNR Improvement of SAR Image

A. Principle of SAR Imaging

In order to analyze the improvement of the SNR of SAR image by the method proposed in this article, we first briefly introduce the principle of SAR imaging algorithm [1].

The LFM signal transmitted by radar can be written as

$$s_t(t_r) = a_r(t_r)\exp\left(j\pi\gamma {t_r}^2 + j2\pi f_c t_r\right) \tag{24}$$

where $a_r(t_r)$ is the window function of the radar LFM signal, γ is the frequency modulation rate of the signal, and f_c is the carrier frequency of the signal.

The SAR imaging geometric model is shown in Fig. 7, θ_{BW} is the beam width of the radar antenna, the center time of the radar synthetic aperture is the origin O of the slow time t_m, V is the speed of the radar platform A, and X_P is the azimuth coordinate of the target P at any point. The closest distance between the target and the radar is R_0, and the slant distance from the radar antenna phase center to the point target at any t_m is $R(t_m; R_0)$. Then the fundamental frequency echo signal of the point target can be expressed as

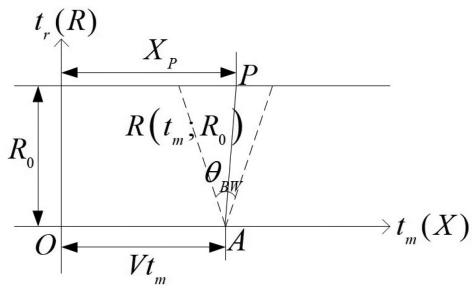

Fig. 7. Geometric configuration of radar and target.

$$s(t_r, t_m; R_0) = a_r\left(t_r - \frac{2R(t_m; R_0)}{c}\right) a_a\left(t_m - \frac{X_P}{V}\right) \times \exp\left[j\pi\gamma\left(t_r - \frac{2R(t_m; R_0)}{c}\right)^2\right] \times \exp\left[-j\frac{4\pi}{\lambda}R(t_m; R_0)\right] \tag{25}$$

where $a_a(t_m)$ is the azimuth window function and $\lambda = c/f_c$ is the wavelength.

If the range window function is a rectangular window, the received signal of (25) after being processed by range matched filtering and range migration compensation can be written as

$$s(t_r, t_m; R_0) = A_1 \sin c\left[\Delta f_r\left(t_r - \frac{2R_0}{c}\right)\right] a_a\left(t_m - \frac{X_P}{V}\right)$$

$$\times \exp\left[-j\frac{4\pi}{\lambda}R\left(t_m;R_0\right)\right] \tag{26}$$

where A_1 is the amplitude of the signal after range pulse compression and Δf_r is the bandwidth of the chirp signal.

Then perform azimuth matched filtering on the echo in (26). If the azimuth window function is also a rectangular window, the echo signal can be rewritten as

$$s\left(t_r,t_m;R_0\right)=A_2\sin c\left[\Delta f_r\left(t_r-\frac{2R_0}{c}\right)\right]\times\sin c\left[\Delta f_a\left(t_m-\frac{X_P}{V}\right)\right]. \tag{27}$$

In (27), A_2 is the amplitude of the point target signal after compression of the range and azimuth and Δf_a is the azimuth Doppler bandwidth of echo.

B. Analysis of Improvement of SNR in CPC–SAR Compared With SNR in Traditional SAR

It can be seen from the above that the SAR imaging algorithm is a 2-D matched filtering process in distance dimension and azimuth dimension. Therefore, we will analyze the improvement of the SNR in SAR image when the CPC method is applied to traditional SAR.

We define the SNR improvement factor of CPC method for SAR image as

$$I=\frac{S/N}{S_0/N_0} \tag{28}$$

where S/N is the SNR at a certain point of the CPC–SAR image, and S_0/N_0 is the SNR at the same point on the traditional radar image.

Due to the presence of noise, the real signal model of the receiving window should be written as

$$\boldsymbol{wx}+\boldsymbol{n}_0=\boldsymbol{r} \tag{29}$$

where $\boldsymbol{n}_0=[n_1,n_2\cdots n_Q]^T$, which represents the noise in any Q continuously distributed receiving windows. Moreover, these noises are generally considered to be Gaussian white noises distributed independently.

Combining (19) and (29), it can be seen that after decoding method is applied to SAR, the power of recovered target echo in CPC–SAR is equal to that in traditional SAR, but the noise signal has changed as follows:

$$\boldsymbol{n}=\left(\boldsymbol{w}^T\boldsymbol{w}\right)^{-1}\boldsymbol{w}^T\boldsymbol{n}_0. \tag{30}$$

Therefore, the improvement factor is only related to the noise power of CPC radar and traditional radar, then (28) can be simplified as

$$I=N_0/N. \tag{31}$$

If the length of range matched filter $\boldsymbol{H}_r$ for SAR imaging is P_r, according to the property of linear convolution, after range dimension matched filtering, the noise σ_{r0} in the traditional SAR and the noise σ_r in the CPC–SAR at any point (t_r,t_m) can be expressed as the inner product of two vectors with length L_r as follows:

$$\begin{aligned}\sigma_{r0}\left(t_r,t_m\right)&=\boldsymbol{H}_r{}^H\boldsymbol{S}_{n0}\left(t_r,t_m\right)\\ \sigma_r\left(t_r,t_m\right)&=\boldsymbol{H}_r{}^H\boldsymbol{S}_n\left(t_r,t_m\right)\end{aligned} \tag{32}$$

where

$$\begin{aligned}\boldsymbol{S}_{n0}\left(t_r,t_m\right)&=\left[s_{n0}\left(t_{r-L_r/2},t_m\right)\cdots\right.\\ &\left.s_{n0}\left(t_r,t_m\right)\cdots s_{n0}\left(t_{r+L_r/2-1},t_m\right)\right]^T\\ \boldsymbol{S}_n\left(t_r,t_m\right)&=\left[s_n\left(t_{r-L_r/2},t_m\right)\cdots\right.\\ &\left.s_n\left(t_r,t_m\right)\cdots s_n\left(t_{r+L_r/2-1},t_m\right)\right]^T.\end{aligned} \tag{33}$$

In (33), $\boldsymbol{S}_{n0}(t_r,t_m)$ and $\boldsymbol{S}_n(t_r,t_m)$ are the noise sampled signal with length L_r and centered at point t_r in the received echo at a certain slow time t_m in traditional SAR and CPC–SAR, respectively.

Similarly, if the length of the azimuth dimension matched filter $\boldsymbol{H}_a$ is L_a, according to the nature of linear convolution, the echo after distance-dimensional matched filtering is then subjected to azimuth-dimensional matched filtering. At any point, the noise σ_{a0} in the traditional SAR and the noise σ_a in the CPC–SAR can also be expressed as the inner product of two vectors of length L_a as follows:

$$\begin{aligned}\sigma_{a0}\left(t_r,t_m\right)&=\boldsymbol{H}_a{}^H\boldsymbol{\sigma}_{r0}\left(t_r,t_m\right)\\ \sigma_a\left(t_r,t_m\right)&=\boldsymbol{H}_a{}^H\boldsymbol{\sigma}_r\left(t_r,t_m\right)\end{aligned} \tag{34}$$

where

$$\begin{aligned}\boldsymbol{\sigma}_{r0}\left(t_r,t_m\right)&=\left[\sigma_{r0}\left(t_r,t_{m-L_a/2}\right)\cdots\right.\\ &\left.\sigma_{r0}\left(t_r,t_m\right)\cdots\sigma_{r0}\left(t_r,t_{m+L_a/2-1}\right)\right]^T\\ \boldsymbol{\sigma}_r\left(t_r,t_m\right)&=\left[\sigma_r\left(t_r,t_{m-L_a/2}\right)\cdots\right.\\ &\left.\sigma_r\left(t_r,t_m\right)\cdots\sigma_r\left(t_r,t_{m+L_a/2-1}\right)\right]^T.\end{aligned} \tag{35}$$

In (35), $\boldsymbol{\sigma}_{r0}$ and $\boldsymbol{\sigma}_r$ are azimuth noise signals with (t_r,t_m) as the center time and length L_a in traditional SAR and CPC–SAR, respectively, which can be calculated by (32).

The ratio of noise power on the traditional SAR and CPC–SAR images can be calculated by (31) and (34). So the SNR improvement factor of the CPC method can be written as

$$\begin{aligned}I&=\frac{E\left[\left|\sigma_{a0}\left(t_r,t_m\right)\right|^2\right]}{E\left[\left|\sigma_a\left(t_r,t_m\right)\right|^2\right]}\\ &=\frac{E\left[\boldsymbol{\sigma}_{r0}{}^H\left(t_r,t_m\right)\boldsymbol{H}_a\boldsymbol{H}_a{}^H\boldsymbol{\sigma}_{r0}\left(t_r,t_m\right)\right]}{E\left[\boldsymbol{\sigma}_r{}^H\left(t_r,t_m\right)\boldsymbol{H}_a\boldsymbol{H}_a{}^H\boldsymbol{\sigma}_r\left(t_r,t_m\right)\right]}.\end{aligned} \tag{36}$$

In addition, according to the characteristics of the azimuth matched filter, it can be deduced that $\boldsymbol{H}_a\boldsymbol{H}_a{}^H$ is an identity matrix. Therefore, (36) can be simplified as

$$I=\frac{E\left[\boldsymbol{\sigma}_{r0}{}^H\left(t_r,t_m\right)\boldsymbol{\sigma}_{r0}\left(t_r,t_m\right)\right]}{E\left[\boldsymbol{\sigma}_r{}^H\left(t_r,t_m\right)\boldsymbol{\sigma}_r\left(t_r,t_m\right)\right]}. \tag{37}$$

We can obtain the relationship between the noise signal $s_n(t_r, t_m)$ in the complete echo recovered by the CPC–SAR at any time and the noise signal $s_{n0}(t_r, t_m)$ of the traditional SAR according to (30). So the relationship between $\boldsymbol{S}_{n0}(t_r, t_m)$ and $\boldsymbol{S}_n(t_r, t_m)$ in (33) is as follows:

$$\boldsymbol{S}_n\left(t_r, t_m\right) = A\left(t_r, t_m\right)\boldsymbol{S}_{n0}\left(t_r, t_m\right) \tag{38}$$

where

$$A\left(t_r, t_m\right) = \begin{bmatrix} a_1\left(t_r, t_m\right) & 0 & \cdots & 0 \\ 0 & a_2\left(t_r, t_m\right) & \cdots & \vdots \\ \vdots & \vdots & \ddots & 0 \\ 0 & \cdots & 0 & a_{L_r}\left(t_r, t_m\right) \end{bmatrix}. \tag{39}$$

The improvement matrix $A(t_r, t_m)$ in (39) is a diagonal matrix, and the elements on the main diagonal are uniquely determined by (30).

Then we substitute (39) into (32), then (32) can be rewritten as

$$\begin{aligned} \sigma_{r0}\left(t_r, t_m\right) &= \boldsymbol{H}_r{}^H \boldsymbol{S}_{n0}\left(t_r, t_m\right) \\ \sigma_r\left(t_r, t_m\right) &= \boldsymbol{H}_r{}^H A\left(t_r, t_m\right)\boldsymbol{S}_{n0}\left(t_r, t_m\right). \end{aligned} \tag{40}$$

Therefore, after distance-dimensional matched filtering, the noise power of the traditional SAR and the noise power of the CPC–SAR can be expressed as

$$\begin{aligned} E\left[\left|\sigma_{r0}\left(t_r, t_m\right)\right|^2\right] &= E\left[\boldsymbol{S}_{n0}(t_r, t_m)^H \boldsymbol{S}_{n0}\left(t_r, t_m\right)\right] \\ E\left[\left|\sigma_r\left(t_r, t_m\right)\right|^2\right] &= E\left[\left(A\left(t_r, t_m\right)\boldsymbol{S}_{n0}\left(t_r, t_m\right)\right)^H \right. \\ &\quad \left. \times A\left(t_r, t_m\right)\boldsymbol{S}_{n0}\left(t_r, t_m\right)\right]. \end{aligned} \tag{41}$$

If we set the variance of independently distributed Gaussian white noise signal $\boldsymbol{S}_{n0}(t_r, t_m)$ as ${\sigma_N}^2$, then (41) can be rewritten as

$$\begin{aligned} E\left[\left|\sigma_{r0}\left(t_r, t_m\right)\right|^2\right] &= L_r {\sigma_N}^2 \\ E\left[\left|\sigma_r\left(t_r, t_m\right)\right|^2\right] &= tr\left[A^H\left(t_r, t_m\right)A\left(t_r, t_m\right)\right]{\sigma_N}^2 \end{aligned} \tag{42}$$

where $tr[A^H(t_r, t_m)A(t_r, t_m)]$ is the trace of $A^H(t_r, t_m)$ $A(t_r, t_m)$, which can be expressed as

$$\begin{aligned} tr\left[A^H\left(t_r, t_m\right)A\left(t_r, t_m\right)\right] &= \left|a_1\left(t_r, t_m\right)\right|^2 + \left|a_2\left(t_r, t_m\right)\right|^2 \\ &\quad + \cdots + \left|a_{L_r}\left(t_r, t_m\right)\right|^2. \end{aligned} \tag{43}$$

Finally, substituting (42) and (35) into (37) can get the final value of improvement factor I, which can be written as

$$I = \frac{L_a L_r}{\sum_{i=-L_a/2}^{L_a/2-1} tr\left[A^H\left(t_r, t_{m+i}\right)A\left(t_r, t_{m+i}\right)\right]}. \tag{44}$$

Its decibel value can be expressed as

$$\begin{aligned} I_{dB} &= 10\log_{10}(L_a L_r) \\ &\quad - 10\log_{10}\left\{\sum_{i=-L_a/2}^{L_a/2-1} tr\left[A^H\left(t_r, t_{m+i}\right)A\left(t_r, t_{m+i}\right)\right]\right\}. \end{aligned} \tag{45}$$

It can be known from (45) that when the length of the matched filter of the distance dimension and the azimuth dimension are fixed, the change of the SNR in SAR image after CPC is only related to the corresponding improvement matrix $A(t_r, t_m)$. The improvement matrix $A(t_r, t_m)$ reflects the accumulation of the echo energy of multiple pulses by the echo decoding method. But this accumulation is not directly superimposed on the echo signal of multiple pulses. Actually, it can be seen from (38) and (39) that the improvement matrix only represents the change of the noise power, so the accumulation here does not change the energy of the target signal, but reduces the energy of the noise to achieve the purpose of improving the SNR of the radar image.

C. Analysis of Improvement of SNR in CPC–SAR Compared With SNR in Traditional Coding SAR

Similarly, referring to (28), we define the improvement factor of SNR in CPC–SAR image compared with SNR in traditional coding SAR image as

$$I' = \frac{S/N}{S_T/N_T} \tag{46}$$

where S/N is the SNR at a certain point of the CPC–SAR image, and S_T/N_T is the SNR at the same point on the traditional coding SAR image.

As shown in Fig. 5, the traditional coding method directly superimposes multiple complete echo signals recovered in a pulse train repetition period in the range dimension and the CPC method accumulates them in the azimuth direction. Therefore, the signal energy in the final imaging result of the two coding methods is the same, then (46) can be simplified as

$$I' = \frac{N_T}{N}. \tag{47}$$

Referring to (33), $\boldsymbol{S}'_n(t_r, t_m)$ is the noise sampled signal with length L_r and centered at point t_r in the received echo at a certain slow time t_m in traditional coding SAR

$$\begin{aligned} \boldsymbol{S}_n{}'\left(t_r, t_m\right) = &\left[s_n{}'\left(t_{r-L_r/2}, t_m\right)\cdots\right. \\ &\left.\times\, s_n{}'\left(t_r, t_m\right)\cdots s_n{}'\left(t_{r+L_r/2-1}, t_m\right)\right]^T. \end{aligned} \tag{48}$$

And referring to (38) and (39), the relationship between $\boldsymbol{S}_{n0}(t_r, t_m)$ and $\boldsymbol{S}'_n(t_r, t_m)$ is as follows:

$$\begin{aligned} &\boldsymbol{S}_n{}'\left(t_r, t_m\right) = A'\left(t_r, t_m\right)\boldsymbol{S}_{n0}\left(t_r, t_m\right) \\ &A'\left(t_r, t_m\right) = \sum_{n_E=1}^{N_E}\left[A'_{n_E}\left(t_r, t_m\right)\right]^H A'_{n_E}\left(t_r, t_m\right) \\ &A'_{n_E}\left(t_r, t_m\right) \\ &= \begin{bmatrix} a'_1\left(t_r, t_m\left(n_E\right)\right) & 0 & \cdots & 0 \\ 0 & a'_2\left(t_r, t_m\left(n_E\right)\right) & \cdots & \vdots \\ \vdots & \vdots & \ddots & 0 \\ 0 & \cdots & 0 & a'_{L_r}\left(t_r, t_m\left(n_E\right)\right) \end{bmatrix} \end{aligned} \tag{49}$$

where N_E is the total number of the recovered echo of traditional coding SAR in one pulse train repetition period. And $A'_{n_E}(t_r, t_m)$ is the improvement matrix corresponding to the $n_E th$ recovered complete echo at azimuth time t_m.

Therefore, combining (49) with (37) and (42), the improvement factor of the CPC method can be written as

$$I' = \frac{\sum_{i=-L_a/2/N_E}^{L_a/2/N_E-1} tr\left[A'^H(t_r, t_{m+i})\, A'(t_r, t_{m+i})\right]}{\sum_{i=-L_a/2}^{L_a/2-1} tr\left[A^H(t_r, t_{m+i})\, A(t_r, t_{m+i})\right]}. \quad (50)$$

It should be noted that when the same number of pulse coding signals are transmitted in the azimuth, the number of azimuth echoes finally imaged by the CPC–SAR is N_E times that of the traditional coding SAR. Therefore, the number of points of the azimuth matched filter of the traditional coding SAR in (50) is L_a/N_E.

Its decibel value can be expressed as

$$\begin{aligned} I'_{dB} &= 10\log 10 \\ &\times \left(\sum_{i=-L_a/2/N_E}^{L_a/2/N_E-1} tr\left[A'^H(t_r, t_{m+i})\, A'(t_r, t_{m+i})\right]\right) \\ &-10\log 10\left(\sum_{i=-L_a/2}^{L_a/2-1} tr\left[A^H(t_r, t_{m+i})\, A(t_r, t_{m+i})\right]\right). \end{aligned} \quad (51)$$

It can be seen from (51) that the improvement of the SNR in CPC–SAR compared with the SNR in traditional coding SAR is only related to the improvement matrix corresponding to the two pulse coding signals.

V. Simulation Results

In this section, we will first use the experimental results to illustrate the advantage of the CPC method in this article over the pulse coding method in [35]. Then we carry out the imaging experiments of CPC–SAR and traditional SAR to verify the effectiveness of the method proposed in this article for HSNR–WS imaging.

About the three experimental parameter tables, here are three explanations. First, the value of the echo length $N$is the maximum unambiguous swath width when the traditional SAR at PRF_t of 20 KHz and pulsewidth of 5 μs. Second, because the traditional coding method in [35] requires that the echo of the last subpulse in the current pulse train must be received before the next pulse train repetition period. Therefore, the pulse train repetition frequency PRF_t in Table I is calculated by (52)

$$\mathrm{PRF}_t = 1/\left(T_c + N \cdot T_p\right) \quad (52)$$

where N is the length of the radar echo and $T_c$is the transmitted coding signal length. Third, because both CPC–SAR and traditional coding SAR can recover two sets of complete echoes in one pulse train repetition period, the number of azimuth echo in CPC–SAR is twice as much as that in traditional coding SAR and the value of equivalent PRF PRF_r in CPC–SAR is twice as much as pulse train repetition frequency PRF_t in CPC–SAR according to Fig. 5.

TABLE I
Experimental Parameters for Traditional Coding SAR

Symbol	Parameter	Value
S_t	transmitted signal	S0S0S00S00-S0-S0S00S00
PRF_t	pulse train repetition frequency	7.4 KHz
f_c	carrier frequency	30 GHz
B	bandwidth	60 MHz
V	platform velocity	1500 m/s; 800m/s
T_P	pulse width	5 us
f_s	sampling rate	80 MHz
N	echo length	9
N_a	azimuth echo number	2048

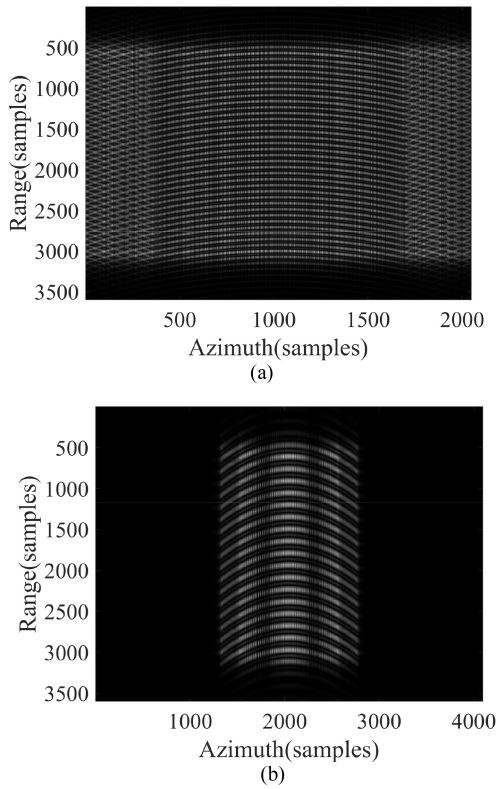

Fig. 8. Range-azimuth two-dimensional spectrum. (a) Spectrum of traditional coding method. (b) Spectrum of CPC method.

A. Simulation Results Comparison of Traditional Coding SAR and CPC–SAR

Fig. 8 is the frequency spectrums of the traditional coding SAR and the CPC–SAR in the range-azimuth dimension. The platform speed of both CPC–SAR and traditional coding SAR is 1500 m/s. It can be seen that the spectrum of the echo signal in the traditional coding SAR is aliased due to the azimuth undersampling, while the CPC–SAR has no spectrum aliasing. This is because the equivalent PRF of the CPC–SAR after

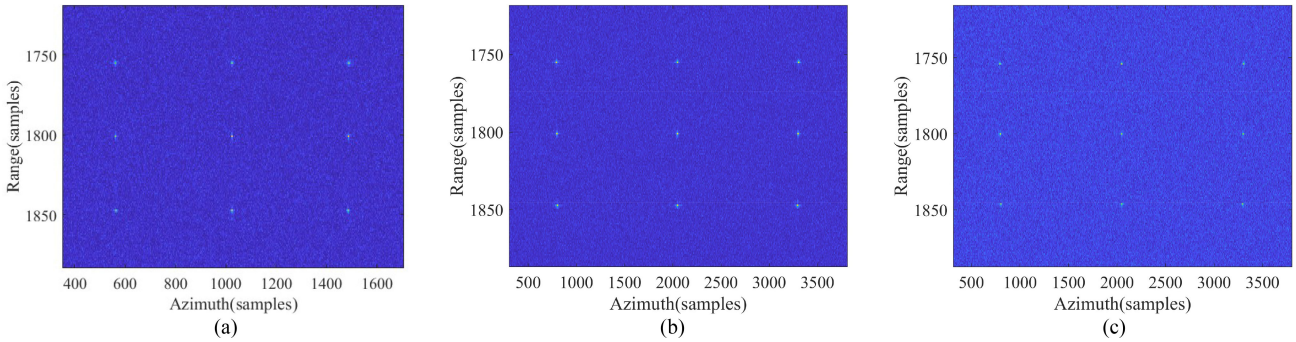

Fig. 9. Point target imaging results. (a) Image of traditional coding SAR. (b) Image of CPC–SAR. (c) Image of traditional SAR.

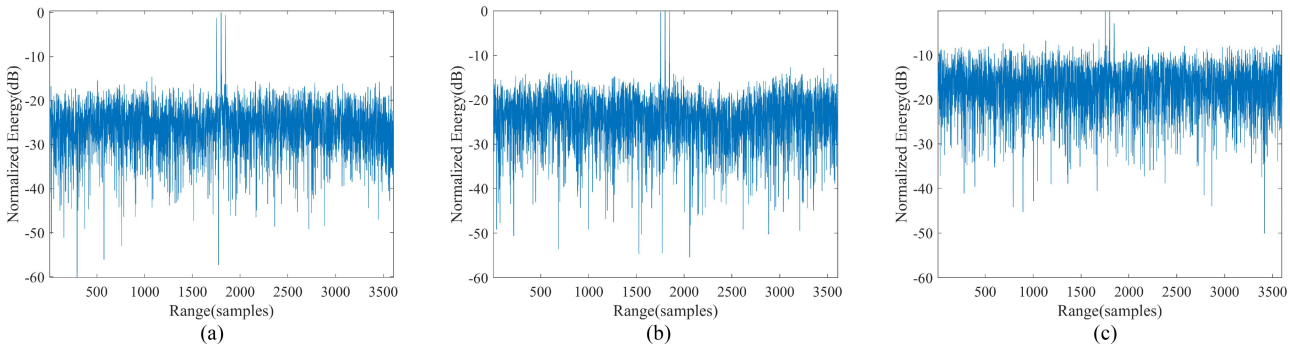

Fig. 10. Range-dimensional profile of point target imaging results at azimuth center time. (a) Image of traditional coding SAR. (b) Image of CPC–SAR. (c) Image of traditional SAR.

decoding is larger than that of the traditional coding SAR as shown in Fig. 5. Therefore, CPC–SAR has a larger unambiguous Doppler bandwidth than traditional coding SAR.

To eliminate spectral aliasing in traditional coding radar so that it has the ability to image normally, we reduce the radar speed to 800 m/s.

Fig. 9(a) and (b) shows the point target imaging results of traditional coding SAR and CPC–SAR, respectively, under the same noise power background. Fig. 10(a) and (b) are the range-dimensional profiles of point target imaging results in traditional coding SAR and CPC–SAR, respectively. And we can obtain the comparison of SNR in the two radar images by Fig. 10(b) and (c) as shown in Fig. 11. It can be seen that the SNR of the two radars are basically the same. This is because the traditional coding method directly superimposes multiple complete echoes recovered in a pulse train repetition period in the range dimension and the CPC method accumulates them in the azimuth direction as shown in Fig. 5. According to (51), the improvement of the SNR of the SAR image by the CPC method compared with the SNR by the traditional coding method is -0.0083 dB.

B. Simulation Results Comparison of Traditional SAR and CPC–SAR

The point/area target imaging results are obtained according to the experimental parameters in Tables II and III.

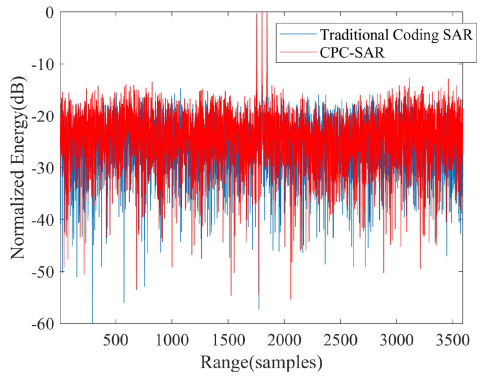

Fig. 11. Range-dimensional profile of point target imaging results at azimuth center time.

Figs. 9(b), (c) and 12 show the imaging results of CPC–SAR and traditional SAR when the noises with same power are added to the original echo. It can be seen that the SNR of the SAR image using CPC method has been significantly improved.

Fig. 10(b)and (c) is the range-dimensional profiles of point target imaging results in CPC–SAR and traditional SAR, respectively. And we can obtain the comparison of SNR in the two radar images by Fig. 10(b) and (c) as shown in Fig. 13. It can be seen that the noise energy of the CPC–SAR is lower than that of the traditional SAR, which indicates that the CPC method

TABLE II
EXPERIMENTAL PARAMETERS FOR CPC–SAR

Symbol	Parameter	Value
S_t	transmitted signal	S0S0S00S00-S0-S0S00S00
PRF_t	pulse train repetition frequency	10 KHz
PRF_r	equivalent PRF	20 KHz
f_c	carrier frequency	30 GHz
B	bandwidth	60 MHz
V	platform velocity	1500 m/s; 800m/s
T_P	pulse width	5 us
f_s	sampling rate	80 MHz
N	echo length	9
N_a	azimuth echo number	4096

TABLE III
EXPERIMENTAL PARAMETERS FOR TRADITIONAL SAR

Symbol	Parameter	Value
S_t	transmitted signal	S
PRF_t	PRF	20 KHz
f_c	carrier frequency	30 GHz
B	bandwidth	60 MHz
V	platform velocity	800 m/s
T_P	pulse width	5 us
f_s	sampling rate	80 MHz
N	echo length	9
N_a	azimuth echo number	4096

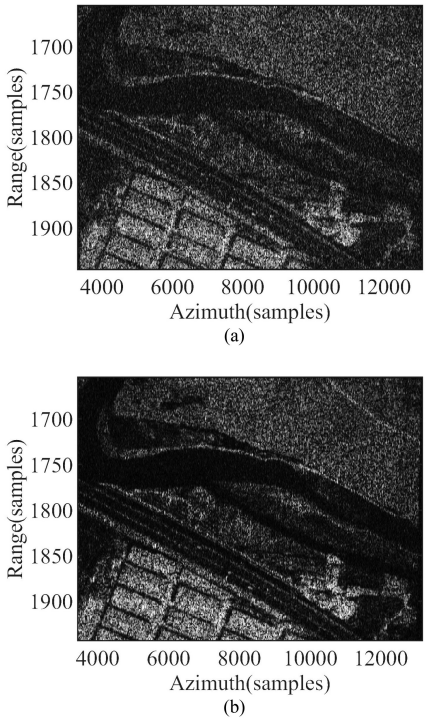

Fig. 12. Imaging results. (a) Image of area target in traditional SAR. (b) Image of area target in CPC–SAR.

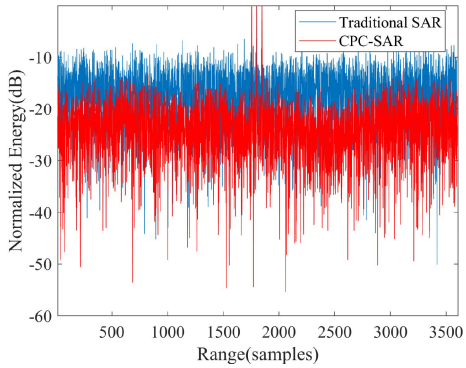

Fig. 13. Range-dimensional profile of point target imaging results at azimuth center time.

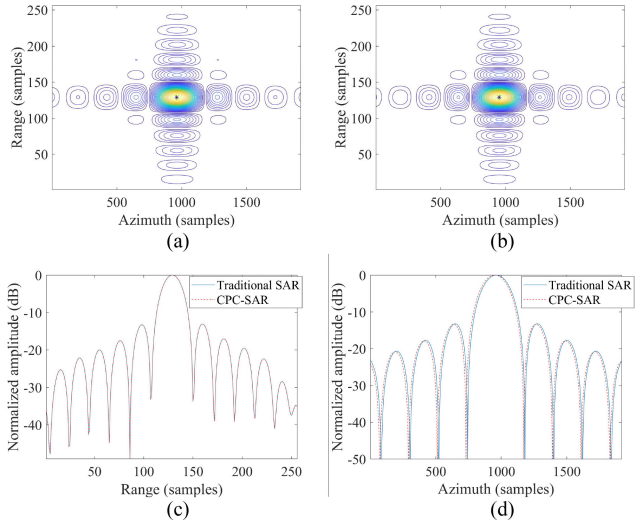

Fig. 14. Image results of scene center point of SAR. (a) Two-dimensional profile of traditional SAR. (b) Two-dimensional profile of CPC–SAR. (c) Range profile. (d) Azimuth profile.

can effectively improve the SNR of the radar echo. Substituting the experimental parameters into (45), we can calculate that the SNR of the radar image is improved by 5 dB, when the CPC method is applied to SAR.

C. Imaging Focusing Quality Evaluation of CPC–SAR

The CPC method can recover the complete echoes and use them to perform SAR imaging. Therefore, in order to evaluate whether this method will affect the focusing effect of radar, we have performed an imaging quality analysis on the center point of the scene in traditional SAR and CPC–SAR. The experimental results are shown in Fig. 14, and the index values used to evaluate the imaging quality of the center point of the scene in Fig. 9(b) and (c) are recorded in Tables IV and V.

By comparing Tables IV and V, we can see that the range and azimuth resolution, the peak sidelobe ratio, and the integral sidelobe ratio of the CPC–SAR point target are basically consistent with them of the traditional SAR, which shows that the

TABLE IV
TRADITIONAL SAR IMAGE QUALITY EVALUATION OF CENTER POINT

Symbol	Parameter	Value
ρ_r	range resolution	2.34 m
ρ_a	azimuth resolution	2.37 m
$PSLR_r$	PSLR of range	-13.04 dB
$PSLR_a$	PSLR of azimuth	-13.17dB
$ISLR_r$	ISLR of range	-10.30dB
$ISLR_a$	ISLR of azimuth	-10.80 dB

TABLE V
CPC–SAR IMAGE QUALITY EVALUATION OF CENTER POINT

Symbol	Parameter	Value
ρ_r	range resolution	2.34 m
ρ_a	azimuth resolution	2.39 m
$PSLR_r$	PSLR of range	-13.04 dB
$PSLR_a$	PSLR of azimuth	-13.34dB
$ISLR_r$	ISLR of range	-10.30dB
$ISLR_a$	ISLR of azimuth	-11dB

CPC method will not affect the focusing effect on the scattered points of radar.

VI. CONCLUSION

This article proposes a novel pulse coding and decoding method to achieve HSNR–WS imaging of SAR. This coding method uses multipulse signals to increase the average transmit power of the radar, and uses the form of coding signal and the swath width of radar to determine the decoding scheme for complete echo recovery. And the recovered echoes can be equivalent to the echoes received by the traditional SAR transmitting a pulse signal with higher peak power without affecting the swath width of radar. Experimental results verify the effectiveness of the proposed CPC method. In the following study, we will make a research on the optimization design of the CPC signal to make the SNR of SAR imaging best and conduct an in-depth study on the signal waveform coding method to improve various performances in SAR system.

REFERENCES

[1] Z. Bao, M. D. Xing, and T. Wang, *Radar Imaging Technique*. Beijing, China: Publish House Electron. Ind., 2005.

[2] L. F. Ding, F. L. Geng, and J. F. Chen, *Radar Principle*. Xi'an, China: Xidian Univ. Press, 2002.

[3] M. Suess, B. Grafmueller, and R. Zahn, "A novel high resolution, wide swath SAR system," in *Proc. IEEE Int. Geosci. Remote Sens. Symp.*, Jul. 2001, pp. 1013–1015.

[4] G. Krieger, N. Gebert, and A. Moreira, "Multidimensional waveform encoding: A new digital beamforming technique for synthetic aperture radar remote sensing," *IEEE Trans. Geosci. Remote Sens.*, vol. 46, no. 1, pp. 31–46, Dec. 2007.

[5] C. Fischer, C. Schaefer, and C. Heer, "Technology development for the HRWS (high resolution wide swath) SAR," in *Proc. Int. Radar Symp.*, 2007, pp. 663–666.

[6] J. J. Zhang, "Study on key techniques of MIMO-SAR," Ph.D. dissertation, Dept. Elect. Eng., Xidian Univ., Xi'an, China, 2014.

[7] Q. S. Wu, H. Z. Shi, M. D. Xing, and Z. Bao, "High signal to noise ratio and high resolution wide swath imaging," *Acta Aeronautica Astronautica Sinica*, vol. 31, no. 5, 2010, Art. no. 1186.

[8] X. N. Zeng, J. Bai, M. L. Hao, and Y. S. Zhang, "High signal to noise ratio and high resolution wide swath imaging of MIMO-SAR based on alamouti space-time encoding," *Acta Electronica Sinica*, vol. 42, no. 6, 2014, Art. no. 1186.

[9] Z. Tang, Y. Deng, R. Wang, and H. Zheng, "Intermittent sampling deceptive jamming suppression for SAR based on azimuth phase coding," in *Proc. IGARSS IEEE Int. Geosci. Remote Sens. Symp.*, Jul. 2019, pp. 513–516.

[10] Q. Q. Feng, H. P. Xu, Z. F. Wu, and B. Sun, "Deceptive jamming suppression for SAR based on time-varying initial phase," in *Proc. IEEE Int. Geosci. Remote Sens. Symp.*, Jul. 2016, pp. 4996–4999.

[11] L. Wei, Y. Lin, and G. Xu, "A new method of phase-perturbed LFM chirp signals for SAR ECCM," in *Proc. China Int. SAR Symp.*, Oct. 2018, pp. 1–4.

[12] Z. Liu, J. Sui, Z. Wei, and X. Li, "A sparse-driven anti-velocity deception jamming strategy based on pulse-Doppler radar with random pulse initial phases," *Sensors*, vol. 18, no. 4, 2018, Art. no. 1249.

[13] M. Soumekh, "SAR-ECCM using phase-perturbed LFM chirp signals and DRFM repeat jammer penalization," *IEEE Trans. Aerosp. Electron. Syst.*, vol. 42, no. 8, pp. 191–205, Feb. 2006.

[14] J. Y. Li and J. G. Wang, "The anti-jamming technology for SAR cheat jamming using complex modulated LFM signal," *J. Electron. Inf. Technol.*, vol. 30, no. 9, pp. 2111–2114, 2008.

[15] X. Z. Feng and X. J. Xu, "Study of countermeasures to deceptive jamming using random linear modulation frequency ratio SAR," *Syst. Eng. Electron.*, vol. 31, no. 1, pp. 69–73, 2009.

[16] Z. Dong, W. Li, and D. N. Liang, "Anti-jamming method based on transmitted signal with random initial phase and chirp rate polarity jittered for SAR," *SIGNAL Process.*, vol. 24, no. 3, pp. 487–490, Jun. 2008.

[17] Z. F. Zhao, "SAR anti-jamming based on waveform design," M.S. thesis, Dept. Sch. Electron. Sci., National Univ. Defense Technol., Changsha, China, 2007.

[18] J. Schuerger and D. Garmatyuk, "Multifrequency OFDM SAR in presence of deception jamming," *EURASIP J. Adv. Signal Process.*, vol. 2010, 2010, Art. no. 451851.

[19] R. J. Wang, J. Chen, X. Wang, and B. Sun, "High-performance anti-retransmission deception jamming utilizing range direction multiple input and multiple output (MIMO) synthetic aperture radar (SAR)," *Sensors*, vol. 17, no. 1, 2017, Art. no. 123.

[20] X. Wang, G. Zhang, Q. Song, and F. Wen, "ECCM schemes against deception jamming using OFDM radar with low global PAPR," *Sensors*, vol. 20, no. 7, 2020, Art. no. 2071.

[21] Y. Li, J. Wang, and X. D. Liang, "Design of MIMO-SAR anti-multipath waveform based on OFDM," *Radar Sci. Technol.*, vol. 17, no. 1, pp. 70–76, 2019.

[22] W. Z. Yue, Y. Zhang, Y. M. Liu, and J. W. Xie, "Radar constant-modulus waveform design with prior information of the extended target and clutter," *Sensors*, vol. 16, no. 6, Jun. 2016, Art. no. 889.

[23] S. M. Karbasi, A. Aubry, and M. H. Bastani, "Robust transmit code and receive filter design for extended targets in clutter," *IEEE Trans. Signal Process.*, vol. 63, no. 8, pp. 1965–1976, Apr. 2015.

[24] S. P. Lu, "Knowledge-based radar target detection and waveform design algorithms," Ph.D. dissertation, Dept. Elect. Eng., Univ. Electron. Sc. Technol., Chengdu, China, 2018.

[25] J. Wang, X. D. Liang, L. Y. Chen, L. N. Wang, and K. Li, "First demonstration of joint wireless communication and high-resolution SAR imaging using airborne mimo radar system," *IEEE Trans. Geosci. Remote Sens.*, vol. 57, no. 9, pp. 6619–6632, May 2019.

[26] J. G. Yang, X. T. Huang, J. Tian, and J. Thompson, "Synthetic aperture radar imaging using stepped frequency waveform," *IEEE Trans. Geosci. Remote Sens.*, vol. 50, no. 5, pp. 2026–2036, Nov. 2012.

[27] Y. Liu, T. Huang, H. Meng, and X. Wang, "Fundamental limits of hrr profiling and velocity compensation for stepped-frequency waveforms," *IEEE Trans. Signal Process.*, vol. 62, no. 17, pp. 4490–4504, Jul. 2013.

[28] Y. M. Liu, H. D. Meng, G. Li, and X. Q. Wang, "Velocity estimation and range shift compensation for high range resolution profiling in stepped-frequency radar," *IEEE Geosci. Remote Sens. Lett.*, vol. 7, no. 4, pp. 791–795, May 2010.

[29] W. Xu, P. P. Huang, and W. X. Tan, "Air-borne linear frequency modulation range interrupted continuous-wave SAR for high-resolution imaging," *J. Eng.*, vol. 2019, no. 19, pp. 5614–5618, 2019.

[30] C. H. Wang, J. W. Xu, G. S. Liao, X. F. Xu, and Y. H. Zhang, "A range ambiguity resolution approach for high-resolution and wide-swath SAR imaging using frequency diverse array," *IEEE J. Sel. Topics Signal Process.*, vol. 11, no. 2, pp. 336–346, Sep. 2017.
[31] J. Wang, X. D. Liang, L. Y. Chen, and K. Li, "A novel space-time coding scheme used for MIMO-SAR systems," *IEEE Geosci. Remote Sens. Lett.*, vol. 12, no. 7, pp. 1556–1560, Mar. 2015.
[32] C. Lin, P. Huang, W. Wang, Y. Li, and J. Xu, "Unambiguous signal reconstruction approach for sar imaging using frequency diverse array," *IEEE Geosci. Remote Sens. Lett.*, vol. 14, no. 9, pp. 1628–1632, Aug. 2017.
[33] Y. Zhou, W. Wang, Z. Chen, Q. Zhao, and R. Wang, "High-resolution and wide-swath SAR imaging mode using frequency diverse planar array," *IEEE Geosci. Remote Sens. Lett.*, vol. 14, no. 9, pp. 321–325, Feb. 2020.
[34] X. N. Zeng, J. Bai, M. L. Hao, and Y. S. Zhang, "High signal to noise ratio and high resolution wide swath imaging of MIMO-SAR based on alamouti space-time encoding," *Acta Electronica Sinica*, vol. 42, no. 6, 2014, Art. no. 1186.
[35] Y. F. Wang, H. P. Li, and S. Han, "The theory and method of pulse coding for radar and its applications," *J. Radars*, vol. 8, no. 1, pp. 1–16, 2019.

Jingyi Wei (Student Member, IEEE) was born in Shaanxi, China, in 1997. She received the B.S. degree in remote sensing science and technology from Xidian University, Xi'an, China, in 2018. She is currently working toward the Ph.D. degree in electronic science and technology with the National Laboratory of Radar Signal Processing, Xidian University.

Her research interests include radar waveform coding and radar anti-jamming.

Yachao Li (Member, IEEE) was born in Jiangxi Province, China, in May 1981. He received M.S. and Ph.D. degrees in electrical engineering from Xidian University, Xi'an, China, in 2005 and 2008, respectively.

He is currently a Professor with Xidian University. His research interests include SAR/ISAR imaging, missile-borne SAR imaging, ground moving target indication, matching and orientation of SAR image, real-time signal processing based on FPGA and DSP technology, and distributed radar.

Rui Yang received the Ph.D. degree in electromagnetic fields and microwave technology from Xidian University, Xi'an, China, in 2008.

He joined the School of Electronic Engineering, Xidian University, in 2008, and was promoted to an Associate Professor in 2012 and a Professor in 2017. From 2009 to 2011, he visited Queen Mary, University of London, London, U.K., as a Newton Research Fellow. His research interests include the electromagnetic metamaterials and their applications in the microwave circuits and antennas.

Prof. Yang was a recipient of the Newton International Fellowship.

Lianghai Li was born in Inner Mongolia, China. He received the B.S. degree in electronic engineering from Inner Mongolia University, Hohhot, China, in 1987, and the M.S. degree in test and metrology technology and instruments from the China Academy of Launch Vehicle Technology, Beijing, China, in 1990.

He is currently the Director of the Beijing Research Institute of Telemetry and the Director of the Precision Guidance and Information Warfare R&D Center in the China Aerospace Science and Technology Corporation. His research interests include test measurement technology and instrument, radar system design, and precision guidance.

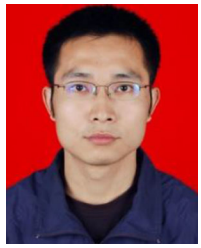

Liang Guo (Member, IEEE) was born in Henan, China, in 1983. He received the B.S. degree in information countermeasure technology from Xidian University, Xi'an, China, in 2005, and the Ph.D. degree in signal and information processing from Xidian University, Xi'an, China, in 2009.

He is currently a Full Professor with the School of Physics and Optoelectronic Engineering, Xidian University. He has authored or coauthored more than 20 papers. His research interests include imaging of several synthetic aperture radar modes, synthetic aperture radar, and real-time imaging.